Surface profile measuring system based on fringe projection and sinusoidal phase modulation

Feng Fan, Duan Fajie, Bo En, Lv Changrong, Fu Xiao, Huang Tingting

(State Key Lab of Precision Measuring Technology & Instruments, Tianjin University, Tianjin 300072, China)

Abstract: A fiber-optic interferometer based on fringe projection and sinusoidal phase modulation (SPM) for three-dimensional surface profile measurement was presented. It made use of Young's double pinhole interference principle to achieve fringe projection. And sinusoidal phase modulation was accomplished by driving piezoelectric transducer using a cosine voltage single. To eliminate the external disturbances such as mechanical vibration and temperature fluctuation, a phase control system was proposed by detecting the phase drift and giving real-time compensation. The phase error was reduced to 6.8 mrad after compensating. A high phase stability of the interference fringe can be achieved. By measuring the surface profile of a glass plate for two times over an interval of 10 min, the repeatability is about 0.05 wave. Experimental results show that the proposed interferometer can be used for surface profile measurement with a high precision.

Key words: surface profile measurement; fringe projection; SPM; phase compensation

CLC number: TH741;O436;TN249 **Document code:** A **Article ID:** 1007-2276(2015)12-3762-07

基于条纹投射和正弦相位调制的表面形貌测量系统

冯 帆,段发阶,伯 恩,吕昌荣,傅 骁,黄婷婷

(天津大学 精密测试技术及仪器国家重点实验室,天津 300072)

摘 要: 基于条纹投射和正弦相位调制技术,提出了一种用于测量物体表面三维形貌信息的光纤干涉系统。通过杨氏双孔结构实现了条纹投射,并以余弦电压信号驱动压电陶瓷实现正弦相位调制。为了消除机械振动、温度波动等外部干扰,采用相位控制系统对相位漂移进行检测,并生成实时相位补偿信号。补偿后相位误差可达 6.8 mrad,从而获得高精度的干涉条纹相位稳定度。对待测件的表面轮廓连续测量两次,时间间隔为 10 min,测量重复度达到 0.05 波长。实验结果证明:该系统能够实现较高精度的表面形貌测量。

关键词: 表面形貌测量; 条纹投射; 正弦相位调制; 相位补偿

收稿日期:2015-04-10; **修订日期:**2015-05-12

基金项目:国家"863"计划(2013AA102402);国家自然科学基金(51275349)

作者简介:冯帆(1989-),男,硕士生,主要研究激光测试技术。Email:tjufengfan@163.com

导师简介:段发阶(1968-),男,教授,博士生导师,主要研究测试计量技术及仪器、光纤传感技术等。Email:fjduan@tju.edu.cn

0 Introduction

With the properties like noncontact, nondestructive, high speed and high resolution, three-dimensional(3-D) profilometry has a variety of applications, such as control for intelligent robots, obstacle detection for vehicle guidance, stamping panel geometry checking, and other fields[1-3]. Traditional 3-D profilometry are based on phase techniques and the phase distribution of the surface can be used to measure height information indirectly through perspective geometry and structural parameters of the projection system. And fringe projection can provide a stabilized reference in many practical applications[4-5]. Of the phased techniques currently used, interferometry has been presented and exhaustively studied to measure surface profiles with high accuracy[6-7]. As a typical interferometry, sinusoidal phase modulating (SPM)has advantages of a simple configuration, high precision, strong anti-jamming ability. SPM can be achieved by driving two sinusoidal vibrating piezoelectric transducers(PZT) to effectively decrease measurement errors, improve the signal-to-noise(SNR) and reduce distortion[8-11].

In this paper, a fiber-optic interferometer is described, which makes use of the Young's double pinhole interference principle and Mach-Zehnder interferometer structure[12]. This interferometer, which is insensitive to external disturbances, can produce an accurate cosine fringe projection and measure surface profile with a high precision [13-16]. In Section 2, the optical setup of the system is presented, and the integrating-bucket method and the geometry model [7] are both described, which can develop the relationship between the fringe pattern and the object's surface profile. In Section 3, the phase control system is presented to extract phase and achieve the phase stabilization of interference fringe pattern. In Section 4, an experimental result of the reconstruction of a paper plate will verify the applicability of the proposed method. Some conclusions are drawn in Section 5.

1 Composition and measuring principle

1.1 Optical setup

Figure 1 shows a schematic representation of the fiber-optic fringe projection measuring system. The light source is a He-Ne laser with good coherence. Light from the laser is collimated by a lens and evenly split into the signal arm (b) and reference arm (c) by a 2×2 optical coupler. These two arms are wrapped under slight tension around the cylinder-shaped PZT. Their fibers' end faces align close together, forming the pinholes in a Young's interference, and composing a Mach-Zehnder interferometer, and then supply a high-density interference fringe projection of cosine distribution on the object when satisfying far-field and paraxial condition. The CCD captures the deformed fringe pattern, and finishes the profile reconstruction with some algorithm.

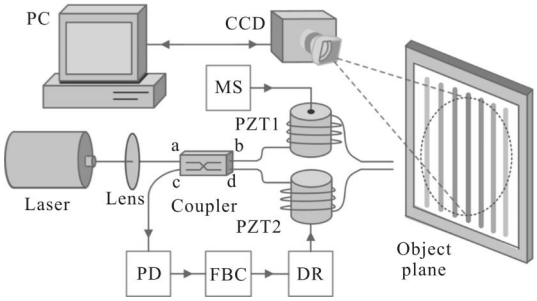

Fig.1 Optical setup of the measuring system (MS, modulated signal; PD, photo detector; FBC, feedback controller; DR, driver)

In addition, the optical fiber exposed in the air is sensitive to external disturbances such as mechanical vibration and temperature fluctuation. These external disturbances cause low frequency fluctuations in the phase of the interference signal. We can eliminate fluctuations in phase by using SPM with a feedback controller. The Fresnel reflections on the two fibers' end faces generate the Michelson interference signal, which travels back through the fiber-optic coupler to the arm (d). This interference signal is projected onto PD, and then transmitted to the feedback controller to generate a compensation single. An oscillator drives PZT1 to produce the phase modulation single and PZT2 is driven

by the compensation voltage. By changing the length of the optical fiber arms, the work of phase stabilization and sinusoidal modulating will be accomplished.

$$M(t)=a\cos(\omega t+\theta) \tag{1}$$

Where a is the amplifier of the modulated signal, ω is the modulation frequency, and θ is the initial phase of $M(t)$. Then the interference fringes are obtained as

$$s(x,y,t)=k_1+k_2\cos[z\cos(\omega t+\theta)+\varphi(x,y)+\xi(t)] \tag{2}$$

where k_1 is the background illumination, k_2 is the contrast between light and dark fringes, z is the phase modulation coefficient, $\varphi(x,y)$ is the phase of the interference fringes, and $\xi(t)$ is the additional phase. The methods to extract $\varphi(x,y)$ and eliminate $\xi(t)$ are described in Sec.3.

1.2 Integrating-bucket method

Figure 2 shows the modulated signal $M(t)$ and the integration of the time-varing signal. The integration is performed in a parallel manner by the CCD. The charge storage period T_C of the image sensor is selected as $T/4$. Then these four separated frames are given by

$$E_p=\frac{4}{T}\int_{(p-1)T/4}^{pT/4} s(x,y,t)\mathrm{d}t \quad (p=1-4) \tag{3}$$

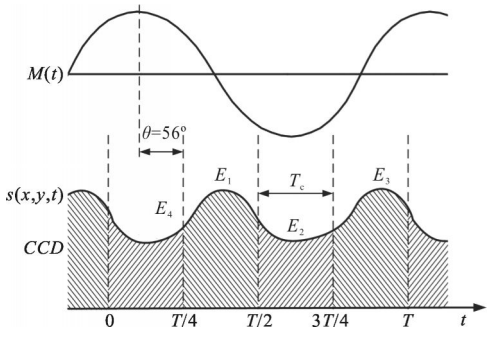

Fig.2 Schematic of the integrating-bucket method

When the parameters z and θ are selected as the optimum values 2.45 and 56° [7], respectively, the influence of the additive noise will decrease to minimum, and the phase $\varphi(x,y)$ is obtained with the simplified formula

$$\varphi(x,y)=\arctan\left(\frac{E_1-E_2-E_3+E_4}{E_1-E_2+E_3-E_4}\right) \tag{4}$$

1.3 Geometry model

The coordinate system of fringe projection model is shown in Fig.3. The plane xoy is chosen as the object plane, and the object plane′s center point O is chosen as the optical model′s origin. The x-axis and y-axis are parallel to the horizontal and vertical direction of the object plane, respectively. The z-axis is along the optical axis of the CCD camera. The center of the CCD lens is located at the point U with a base line distance of d from the origin. The center of the fiber projector is located at the point W. To make sure that UV is parallel to the y-axis, the precise position of W is found, which has a distance of D from the origin. The interference fringes from the fiber projector are aligned along the y-axis with the 0th order fringe, which makes a projection angle of β_0. The coordinates of a point $K(x,y,z)$ on the fringe plane with a projection angle of β satisfies the plane equation given by

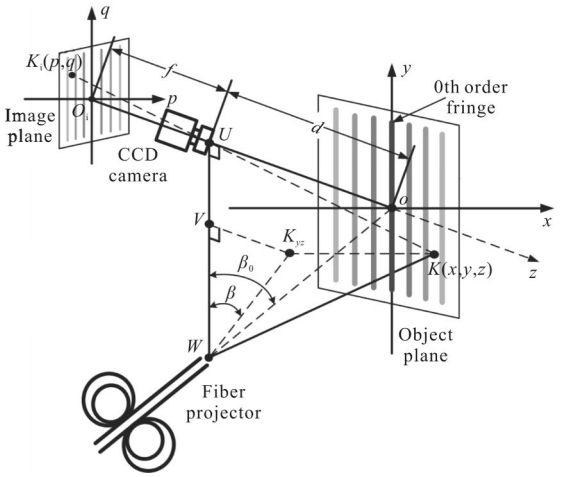

Fig.3 Fiber-optic interference fringe projection model.

$$\sin\beta(\sqrt{D^2-d^2}+y)=\cot\beta(d+z) \tag{5}$$

$K_i(p,q)$ is the mapped point located at the image plane, where p and q are the indices of the horizontal and vertical pixels, respectively. The image point K_i is thus the line projection of point $K(x,y,z)$ to the image plane through the lens center. By defining f as the distance between lens center and image plane, the mapping relation is obtained between K and K_i, which is given by

$$\frac{x}{-p}=\frac{y}{-q}=\frac{d+z}{f} \tag{6}$$

Solving Eqs.(5) and(6) for the coordinate (x,y,z), it is obtained

$$\begin{cases} x=-\dfrac{p\sqrt{D^2-d^2}}{f\cos\beta+q} \\ x=-\dfrac{q\sqrt{D^2-d^2}}{f\cos\beta+q} \\ z=\dfrac{f\sqrt{D^2-d^2}}{f\cos\beta+q}-d \end{cases} \tag{7}$$

The fringe projection angle β is related to the phase $\varphi(x,y)$ of the optical fiber interferometer by

$$\varphi(x,y)=\frac{2\pi}{\lambda}-l_0\tan(\beta-\beta_0)+\varphi_0 \tag{8}$$

where l_0 is the distance separating the two fiber cores, λ is the wavelength of laser, φ_0 is the initial phase difference between two optical arms. Satisfying the far-field and paraxial condition, $\tan(\beta-\beta_0)$ is equivalent to $\beta-\beta_0$ and Eq.(8)can be simplified as

$$\beta=\frac{\lambda}{2\pi l_0}[\varphi(x,y)-\varphi_0]\beta_0 \tag{9}$$

Once the interference phase is determined, Eq.(9)can be used to solve for the projection angle and subsequently to find coordinates $K(x,y,z)$ using Eq.(7).

2 Phase control system

The current in the laser changes by ΔI_T with temperature. The ΔI_T produces a small change in the wavelength of the laser by $k_{\lambda-I}\Delta I_T$, where $k_{\lambda-I}$ represents wavelength-current coefficient. The external mechanical vibration causes the change Δl_V in the optical path difference between the signal and reference waves. These ΔI_T and Δl_V cause phase fluctuation in interference signal. The phase shift will be controlled by driving PZT2 to produce Δl_C. Considering the changes Δl_V, Δl_C, ΔI_T, the initial phase φ_0 and Fresnel reflection signals undergoing a double optical path, the Michelson interference signal for SPM is written as

$$S(t)=k_1+k_2\cos[z\cos(\omega t+\theta)+2\varphi_0+2\xi(t)] \tag{10}$$

where the additional phase is given by

$$\xi(t)=\frac{2\pi}{\lambda}(\Delta l_V+\Delta l_C)-\frac{2\pi l k_{\lambda-I}}{\lambda^2}\Delta I_T \tag{11}$$

The Bessel expansion of Eq.(10) is

$$S(t)=k_1+k_2\cos[\varphi(t)]J_0(z)+2k_2\cos[\varphi(t)]\sum_{n=1}^{\infty}(-1)^nJ_{2n}(z)\cos[2n(\omega t+\theta)]-2k_2\sin[\varphi(t)]\sum_{n=0}^{\infty}(-1)^nJ_{2n+1}(z)\cos[2(2n+1)(\omega t+\theta)] \tag{12}$$

where $\varphi(t)=2\varphi(t)+2\xi(t)$ and $J_{2n}(z)$ is an n-order Bessel function of the first kind

$$J_n(z)=\sum_{m=0}^{\infty}(-1)^n\frac{1}{m!\ (n+m)!}\left(\frac{z}{2}\right)^{n+2m} \tag{13}$$

Figure 4 shows the schematic of the phase control system, which is mainly composed of the following steps. When $S(t)$ is processed by a band-pass filter with a center frequency of 2ω, the second harmonic component is obtained

$$B(t)=2k_2J_2(z)\cos[\varphi(t)]\cos[2(\omega t+\theta)] \tag{14}$$

$B(t)$ is multiplied by the modulated signal $M(t)$, which is as a fundamental carrier. Then we let the results pass a low-pass filter to obtain the low-frequency component.

$$L(t)=ak_2J_2(z)\cos[\varphi(t)] \tag{15}$$

$L(t)$ is divided by its amplitude $|L(t)|$ by the peak detection circuit. Then $\varphi(t)$ can be demodulated by the arccosine calculation.

$$\varphi(t)=\arccos[L(t)/|L(t)|] \tag{16}$$

To eliminate the phase diversity $\varphi(t)$ caused by external disturbances to zero, a DA module is used to generate a compensation voltage

$$L(t)=-k_{P-V}[\varphi(t)] \tag{17}$$

where k_{P-V} is the phase-voltage coefficient. In the phase control system, we can control the phase shift by driving PZT1 with the modulated signal $L(t)$ for SPM and driving PZT2 with the compensation signal $V(t)$ to reduce the additional phase. In this way, the phase of interference

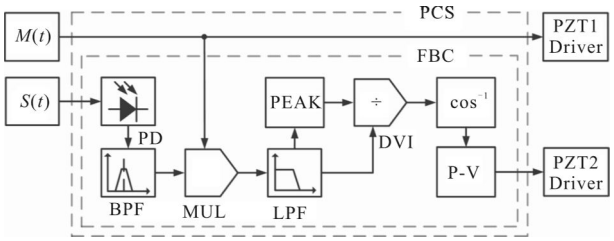

Fig.4 Schematic of the phase control system with feedback controller (PCS, phase control system; BPF, band-pass filter; MUL, multiplication; LPF, low-pass filter; PEAK, peak detection circuit; DVI, division; COS-1, arccosine calculation; P-V, phase to voltage module)

fringes will be well stabilized.

3 Experiment

To summarize the preceding parts, proposed system consist of projecting a fringe pattern onto an object using a fiber −optic interferometer and sinusoidal phase modulation, eliminating external disturbances using the phase control system (Sec.3), obtaining the phase using Eq.(4), and finding surface profile using Eq.(7). To verify our system measuring accuracy, an experiment of measuring the surface profile of a glass plate is carried out. Figure 1 shows the experimental setup, which mainly consists of a He−Ne laser(JDSU 1100, output power 5 mW, wavelength 632.8 nm), a CCD camera (OLYMPUS i−SPEED 3, resolution 1 280 H×1 024 V), and a 3 dB optical coupler(50∶50 split ratio). The SPM frequency for PZT1 is 2 kHz. The modulation depth and the initial phase meet the optimum SPM condition (z=2.45, θ=56°). The center frequency of BPF and the cutoff frequency of LPF are 2 kHz and 200 Hz, respectively. Besides, the standard PZT−8 type of material is applied to PZT1 and PZT2, whose expansion coefficient is 210×10^{-12} C/N.

Due to temperature fluctuation and mechanical vibration, the phase shift always occurs. So in the experiment, firstly the PCS is used to eliminate the external disturbance and accomplish the work of phase stabilization. The phase $\phi(t)$ is measured for 100 times in 10 minutes when the PCS is switched off. $\phi(t)$ fluctuates as shown in Fig.5(a). The maximum phase error is 1 642.89 mrad, and the minimum phase error is 78.53 mrad, respectively. The phase $\phi(t)$ fluctuates with a amplitude of 1 564.36 mrad. Then PCS operating is made, and the phase $\phi(t)$ in 10 minutes is captured in the same way. The residual phase fluctuates from 101.76 mrad to 115.37 mrad as shown in Fig.5(b). Under the adaptive phase control, the compensation voltage nearly eliminates the fluctuations. However, the fluctuation of it is about 13.61 mrad with a bias value 108.56 mrad. So the phase error is less than 6.8 mrad for the fringe map.

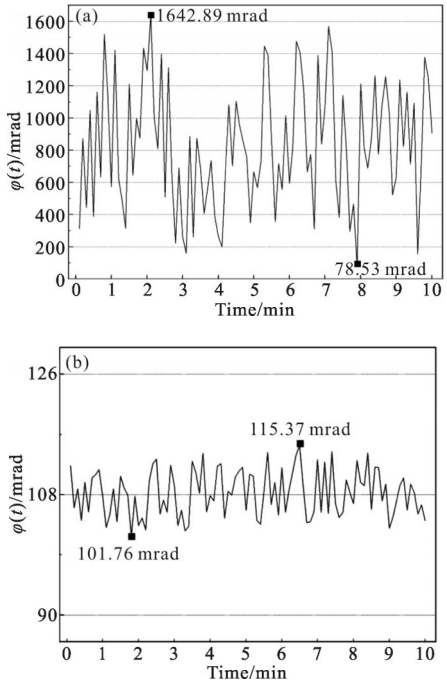

Fig.5 Phase $\phi(t)$ without and with PCS working

When the feedback control voltage is given to the PZT2, the phase of interference fringes will be stabilized in about o.5 ms as shown in Fig.6. By capturing the frequency spectrum of this signal for a few minutes, it is found that the amplitude of the first harmonic is inferior to that of the second harmonic with the minimum value 17.43 dB and maximum value 18.53 dB presented in Fig.7, respectively.

Then the surface profile of a glass plate can be the measured. This system uses a high speed CCD camera with a sampling frequency of 8 kHz to capture the time varying fringes patterns in parallel during the four quarters of one modulation period. A set of four images, which have a small area of interest containing 100 pixel×100 pixel, is shown in Fig.8.

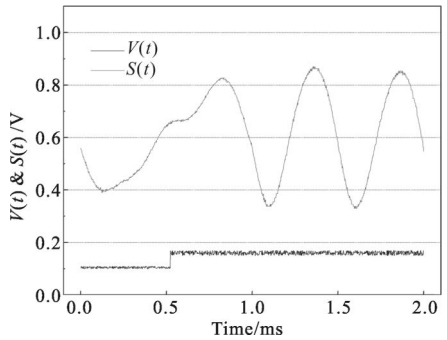

Fig.6 Interference single $S(t)$ with the feedback control

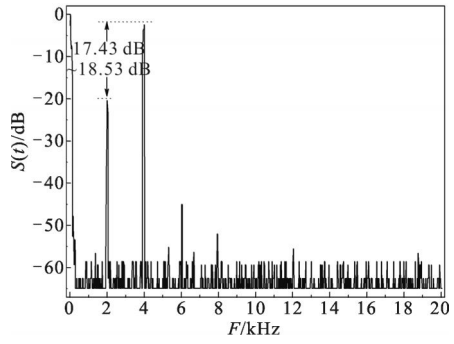

Fig.7 Frequency spectrum of $S(t)$

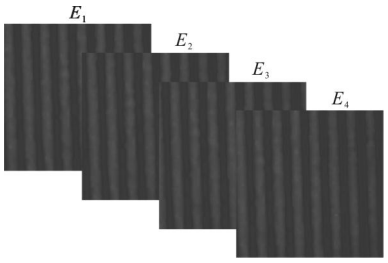

Fig.8 Four fringe patterns captured in one modulation period

Surface profile measurements are demonstrated with the phase control system operating. Fig.9(a)provides the three-dimensional surface profile of the glass plate. In the maps, X and Y are coordinates in units of 10 μm, and Z is the roughness in a unit of nm. In the same way, the second measurement shown in Fig.9(b) is implemented 10 min after the first measurement. To observe the difference in two times profile measurements, two measuring profiles are subtracted for each corresponding pixel as shown in Fig.10. The root mean square error(RMSE) is 0.05 wave,

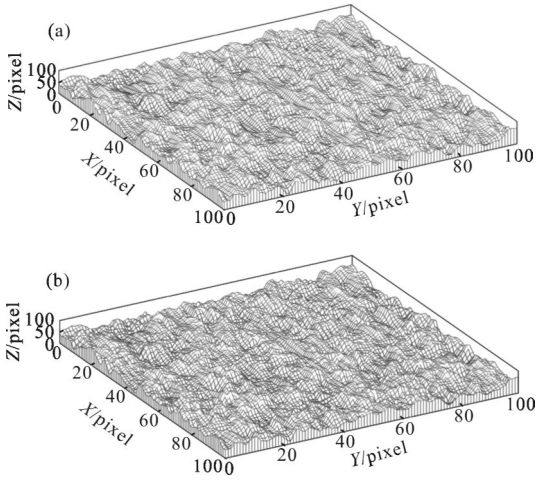

Fig.9 Surface profile of the glass plate and surface profile of the glass plate obtained 10 min later

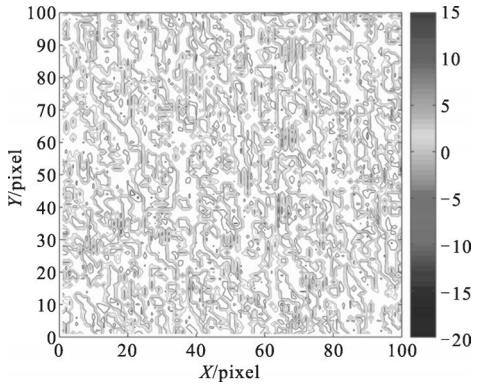

Fig.10 Surface profile measuring difference between Fig.9(a) and(b)

which estimates the repeatability of these measurements.

4 Conclusion

A fiber-optic interferometer is studied based on fringe projection and sinusoidal phase modulation for three-dimensional surface profile measurement. In order to clear away from the outside disturbance, a closed-loop phase control system is built using peak detection method and a disturbance-free performance is achieved by a phase stability of 6.8 mrad. By measuring the surface profile of a glass plate for twice, repeatability is estimated as 0.05 wave. The experimental results show that the proposed profile measuring system can be used for surface profile measurement with a high accuracy and strong anti-interference ability. In the future, a two-wavelength sinusoidal phase-modulating laser wil be used as the light source to increase the measuring range.

References:

[1] Chen F, Brown G M, Song M. Overview of three-dimensional shape measurement using optical methods [J]. ***Optical Engineering***, 2000, 39(1): 10-22.

[2] Robinson D W, Reid G T. Interferogram Analysis, Digital Fringe Pattern Measurement Techniques [M]. Bristol: Institute of Physics Publishing, 1993: 94-140.

[3] Genovese K, Pappalettere C. Whole 3D shape reconstruction of vascular segments under pressure via fringe projection techniques [J]. ***Optics and Lasers in Engineering***, 2006, 44 (12): 1311-1323.

[4] Indebetouw G. Profile measurement using projection of running fringes[J]. ***Applied Optics***, 1978, 17(18): 2930-2933.

[5] Lalor M J, Atkinson J T, Burton D R, et al. A fiber optic computer controlled fringe projection interferometer for surface measurement[C]//Proc Fringe, 1993, 93: 242-247.

[6] Malacara D, Servin M, Malacara Z. Interferogram Analysis for Optical Testing[M]. New York: Marcel Dekker Inc, 1998.

[7] Dubois A. Phase-map measurements by interferometry with sinusoidal phase modulation and four integrating buckets[J]. ***JOSA A***, 2001, 18(8): 1972-1979.

[8] Sasaki O, Okazaki H. Sinusoidal phase modulating interferometry for surface profile measurement[J]. ***Applied Optics***, 1986, 25 (18): 3137-3140.

[9] Sasaki O, Okazaki H, Sakai M. Sinusoidal phase modulating interferometer using the integrating-bucket method [J]. ***Applied Optics***, 1987, 26(6): 1089-1093.

[10] He G, Wang X, Zeng A, et al. Sinusoidal phase-modulating laser diode interferometer for real-time surface profile measurement[J]. ***Chinese Optics Letters***, 2007, 5(3): 164-167.

[11] Sasaki O, Suzuki T, Takahashi K. Sinusoidal phase modulating laser diode interferometer with feedback control system to eliminate external disturbance [J]. ***Optical Engineering***, 1990, 29(12): 1511-1515.

[12] Pennington T L, Xiao H, May R, et al. Miniaturized 3-D surface profilometer using a fiber optic coupler[J]. ***Optics & Laser Technology***, 2001, 33(5): 313-320.

[13] Chung-Feng Jeffrey Kuo, Han-Cheng Wu. A homography fringe generation method of fringe projection profilometry technology[J]. ***Optics and Lasers in Engineering***, 2014, 56: 28-34.

[14] Bo En, Duan Fajie, Lv Changrong, et al. Sinusoidal phase modulating interferometry system for 3D profile measurement [J]. ***Optics & Laser Technology***, 2014, 59: 137-142.

[15] Li Ameng, Peng Xiang, Yin Yongkai, et al. Fringe projection based quantitative 3D microscopy [J]. ***Optik - International Journal for Light and Electron Optics***, 2014, 21: 5052-5056.

[16] Zhou Na, An Zhiyong, Li Yonghao. Large-sized three-dimensional profile measurement technology based on laser radar [J]. ***Infrared and Laser Engineering***, 2011, 40(12): 2465-2468. (in Chinese)
周娜, 安志勇, 李咏豪. 采用激光雷达的大尺寸三维形貌测量技术[J]. 红外与激光工程, 2011, 40(12): 2465-2468.